



Structural stability and magnetism of γ' -Fe₄N and CoFe₃N compounds

X.G. Ma, J.J. Jiang*, P. Liang, J. Wang, Q. Ma, Q.K. Zhang

Department of Electronic Science and Technology, Huazhong University of Science and Technology, Wuhan 430074, China

ARTICLE INFO

Article history:

Received 14 November 2008
Received in revised form 21 January 2009
Accepted 22 January 2009
Available online 6 February 2009

Keywords:

Perovskite nitrides
Magnetism
Total energy
Structural stability

ABSTRACT

Total energy and electronic structure calculations for γ' -Fe₄N and CoFe₃N in the anti-perovskite crystal structure have been performed to understand the structural stability and magnetism using plane-wave pseudopotential method. The virtual crystal approximation (VCA) was used to study order/disorder to examine the effect of the substitution of Co for Fe on the structural stability in CoFe₃N alloy. The results show that CoFe₃N energetically prefers ordered configuration for Co atoms occupying the corner position. Moreover, the substitution of Co for Fe at corner sites does slightly change the lattice constant, whereas it increases bulk modulus and could hardly changes the ductility. To reveal the role of nitrogen in γ' -Fe₄N and CoFe₃N, the Mulliken charge and bond population are used as a measure of charge transfers and an analysis of the covalency of these systems, respectively. It turns out that the further distant atoms from the N atom have the larger magnetic moment for γ' -Fe₄N and CoFe₃N, due to the spin-down electrons transfer from the corner atoms to the face-centered atoms.

© 2009 Published by Elsevier B.V.

1. Introduction

Iron nitride possesses particular magnetic properties that include high saturation magnetization and low coercivity over pure iron and good mechanical and corrosion resistance [1–3]. So it has received much attention as a promising material for several applications, e.g., high density magnetic recording material, hard and wear-resistant materials [4–6]. γ' -Fe₄N belongs to the anti-perovskite crystal structure, where the iron atoms occupy the two nonequivalent sites, namely, the corner (c) sites and face-centered (f) sites, while the nitrogen atoms sit at the body-centered (b) positions. It can also be seen as γ' -Fe (FCC) where nitrogen has been inserted at the b sites. The main roles of nitrogen are discussed in enhancing the iron moment and raising the Curie temperature by Coey and Smith [7], whereas physical origin of the change of magnetic moment for nitrogen doping is still in debate.

In order to improve the corrosion resistance and magnetic properties of γ' -Fe₄N, various elements, e.g., Mn, Ni, Ir, Rh, etc., are used as a substitution for Fe [8,9]. It has been seen that Mn is a valuable substitution for Fe in γ' -Fe₄N because of its control over particle size during the processing [10]. The interest of Ni lies primarily in its improved corrosion resistance over pure γ' -Fe₄N. Also, the substitution of Ni for Fe does not change the saturation magnetization significantly compared to the other substituents such as: Mn, Sn, Ru, Os, Nd, etc., and exhibits better magnetic and electrical properties over pure iron [11]. All of Fe, Mn, Ni and Co belong to 3d

magnetic elements, and are similar in metallic radius. So the magnetic properties of Co ions excite our interest in the effects of the substitution of Co for Fe on the magnetic properties of the γ' -Fe₄N compounds. And the experimental results of Wang et al. showed a very high saturation magnetization of Fe, Co, N films [12]. Until now, it is difficult to obtain ordered CoFe₃N from the experimental studies [13–15].

The aim of the present work is to assess the structural stability, magnetism, the chemical role of nitrogen within γ' -Fe₄N and CoFe₃N and the effect of Co substitution for Fe at the cube c sites. The paper is organized as follows. Section 2 describes some technical details about the model and methodology applied. Section 3 reports and discusses the results. Section 4 draws some conclusions.

2. Calculation model and methods

All calculations were performed in the framework of density functional theory [16] within the generalized gradient approximation (GGA) using the Perdew–Wang (PW91) [17] exchange correlation potential, and utilizing the plane-wave total energy pseudopotential method as implemented in Castep code [17,18]. The ion–electron interaction is modeled by ultrasoft pseudopotential in the Vanderbilt form [19]. Using these methods, satisfactory results have been received in other studies [20,21]. The valence atomic configurations are 3d⁶4s² for Fe, 3d⁷4s² for Co and 2s²2p³ for N atom. For the 5-atom unit-cell calculations, the cutoff energy of plane-waves was set to 400 eV and a k-point mesh 6 × 6 × 6 was used. Geometry optimizations were performed using the Broyden–Fletcher–Goldfarb–Shanno (BFGS) method [22]. Atomic relaxations were considered to be converged when the residual forces were smaller than 5 × 10^{−5} Pa.

Within the ultrasoft pseudopotential method it is possible to formulate a virtual crystal approximation (VCA) which can be used to study order/disorder and solid solutions [23]. This positional disorder is typically manifested in site occupancy factors of less than unity for the average unit cell. In the VCA, atomic sites in a crystal can be described in terms of a hybrid atom that consists of two or more element types. This approach is complementary to the configurational approach in that it does not

* Corresponding author. Fax: +86 27 87544472.

E-mail address: jiangjj@mail.hust.edu.cn (J.J. Jiang).

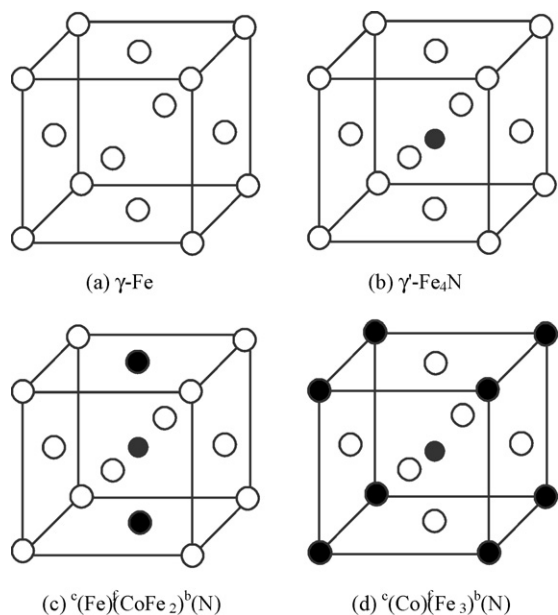


Fig. 1. Crystal structure of γ -Fe, γ -Fe₄N, ${}^c(\text{Fe})^f(\text{CoFe}_2)^b(\text{N})$, ${}^c(\text{Co})^f(\text{Fe}_3)^b(\text{N})$. Large empty spheres: Fe; large black spheres: Co, smaller black spheres: N.

require the use of supercells. The implementation of the VCA follows the description of Bellaiche and Vanderbilt [24]. To understand the effects of the substitution of Co for Fe on structural stability of the γ -Fe₄N, the VCA was used to study order/disorder. For each order/disordered structure, the geometry optimization was first performed to find its ground state, as well as other physical properties. The Mulliken charges and bond populations were investigated using a projection of the plane-wave states onto a linear combination of atomic orbitals (LCAO) basis set [25,26], which is widely used to perform charge transfers and populations analysis.

3. Results and discussion

3.1. Structure stability

We started the geometry optimization of γ -Fe₄N structure with a lattice constant from experiment: $a = 3.790 \text{ \AA}$ [27]. The calculations were carried out for both spin-polarized (SP) and non-spin-polarized (NSP) configurations. The resulting structure was found to be cubic with equilibrium lattice constants: $a_{\text{SP}}(\gamma\text{-Fe}_4\text{N}) = 3.761 \text{ \AA}$, $a_{\text{NSP}}(\gamma\text{-Fe}_4\text{N}) = 3.651 \text{ \AA}$, with an energy difference of $\Delta E(\text{SP-NSP}) = -1.22 \text{ eV}$ per formula unit (f.u.) favoring the SP configuration. Calculated lattice constant of γ -Fe₄N for SP configuration is only 0.7% smaller than the experimental value of 3.790 \AA . To examine the effect of nitrogen on the structure and magnetization of γ -Fe₄N, the structure of γ -Fe for SP configuration was also studied. The lattice parameter a is 3.598 \AA . Due to the N insertion in the b site of γ -Fe, the volume expansion is about 14.2%, which is smaller than the experimental value of Lord's [28].

In order to obtain stable structure of CoFe₃N, we analyzed the atomic ordering of the Fe and Co atoms over the c and f sites. In the VCA a virtual atom is created by taking the average of the atoms occurring at the lattice sites. In the present case an average of Fe and Co is taken for different concentrations x , so the total energies of statistically disordered compounds are designated ${}^c(\text{Co}_x\text{Fe}_{1-x})^f(\text{Co}_{1-x}\text{Fe}_{2+x})^b(\text{N})$. The Wyckoff superscripts indicate the positions in the disordered phase. They are compared with the two ordered configurations: the Co atom may either exclusively replace one of the three facial Fe(f) atoms, ${}^c(\text{Fe})^f(\text{CoFe}_2)^b(\text{N})$ see Fig. 1c and Co may substitute for the corner Fe(c) atoms, ${}^c(\text{Co})^f(\text{Fe}_3)^b(\text{N})$ see Fig. 1d. The numerical results are given in Fig. 2 as relative energies with respect to the ordered configurations, ${}^c(\text{Co})^f(\text{Fe}_3)^b(\text{N})$. At $x = 0.5$, the disordered compound has highest energy, which implies

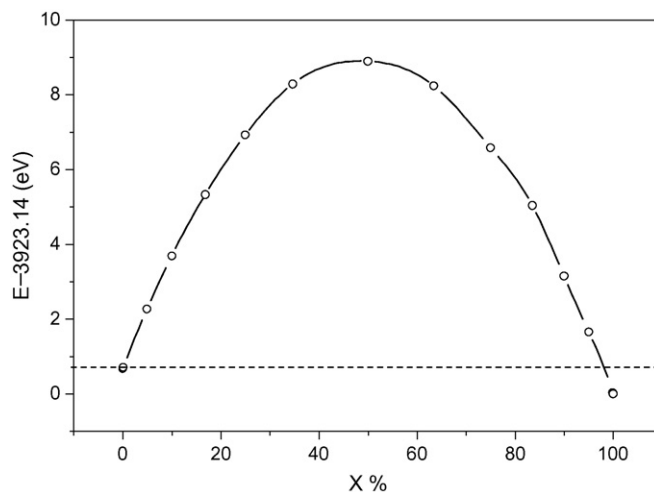


Fig. 2. Total energy as a function of Co concentration x at c sites. The dashed horizontal line indicate the total energy of ${}^c(\text{Fe})^f(\text{CoFe}_2)^b(\text{N})$ structure.

unstable configuration, whereas the two ordered compounds have relative lower energy than disordered one, indicating that they may be stable phase.

The total energy versus volume curve for SP and NSP configurations for the ordered structures mentioned in Fig. 1 are displayed in Fig. 3. The ferromagnetic state (FM) is largely preferred over the nonmagnetic one in the two ordered configurations. The average total energy of the FM ${}^c(\text{Fe})^f(\text{CoFe}_2)^b(\text{N})$ is about 0.178 eV/f.u. higher than that of FM ${}^c(\text{Co})^f(\text{Fe}_3)^b(\text{N})$ at all atomic volumes considered, indicating that CoFe₃N energetically prefers to yield the latter, namely, for Co atoms, the c position is the optimum choice. Two factors, namely, the relative affinity of Co and Fe for nitrogen and the differences in atomic sizes, simply interpret the atomic ordering. The size of the c position is estimated as 1.42 \AA whereas the value for the f site is only 1.28 \AA [29]. Table 1 shows the substitution of Co for Fe(c) do hardly change the lattice constant, due to their similarity of the metallic radius of Co to that of Fe (1.25 \AA). Relative affinity of Co and Fe for nitrogen has little relation the crystal constant, but it has great effect on the magnetic property of the compound. In the following, we only considered this ordered ${}^c(\text{Co})^f(\text{Fe}_3)^b(\text{N})$ configuration ($x = 0$) within the substitution of Co for Fe in γ -Fe₄N.

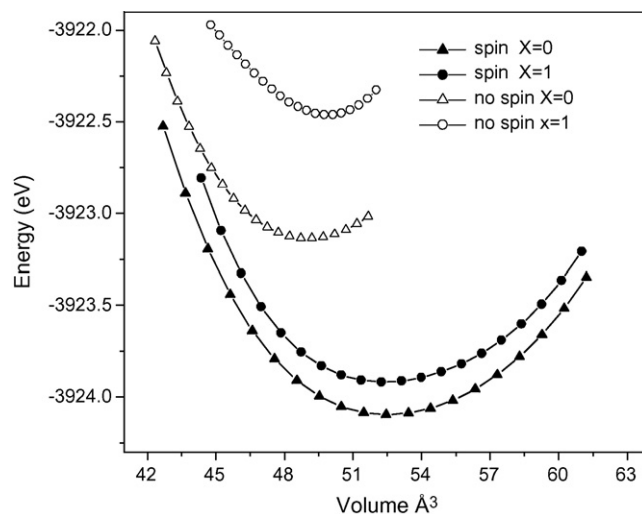


Fig. 3. Total energy of two ordered configurations of ${}^c(\text{Co}_x\text{Fe}_{1-x})^f(\text{Co}_{1-x}\text{Fe}_{2+x})^b(\text{N})$ at $x = 0$ and 1 , respectively. Open symbols denote nonmagnetic state and filled symbols denote the ferromagnetic state.

Table 1

Theoretical lattice constants a (Å), Elastic constants (GPa), effective isotropic elastic moduli (GPa), spin magnetic moment M_s (μ_B /f.u.) and local magnetic moments (μ_B /atom) and total density of states at the Fermi level $N(E_f)$ (in units of states/eV/f.u.) The value in bracket is the magnetic moment of Co atom at F site.

Material	a	c_{11}	c_{12}	c_{44}	B	G	B/G	E	ν	M_s	u_c	u_f	$N(E_f)$
γ -Fe	3.598	68	275	-26	206	-57	-3.6	-188	0.65	10	2.5	2.5	4.0
γ -Co	3.555	274	176	143	209	105	2.0	270	0.28	6.88	1.72	1.72	3.7
γ' -Fe ₄ N	3.761	306	99	47	168	70	2.4	184	0.32	9.76	2.96	2.24	4.6
^c (Fe) ^f (CoFe ₂) ^b (N)	3.732	341	71	49	161	83	1.9	213	0.28	8.20	3.04	2.02 (1.08)	-
^c (Co) ^f (Fe ₃) ^b (N)	3.751	376	118	59	204	87	2.3	229	0.31	8.77	1.76	2.32	5.2

3.2. Elastic constants

The elastic constants were calculated on the basis of the results of the geometry optimization. We obtained all the elastic constants by an application of an appropriate deformation of the unit cell and some estimate of the appropriate effective isotropic modulus. It is well known that the elastic behavior of a cubic crystal is completely described by three independent constants c_{11} , c_{12} , and c_{44} . The bulk modulus B is defined by a linear combination of the elastic constants $B = (c_{11} + 2c_{12})/3$, which represents the resistance to volume change and is related to the overall atomic binding properties in a material, while the shear modulus $G = (c_{11} - c_{12} + 3c_{44})/5$ represents the resistance to plastic deformation. The elastic modulus tensor of an isotropic elastic material has only two independent values, which are usually given as any two of the set: the Young's modulus E , the Poisson's ratio ν , the bulk modulus B , and the shear modulus G . The following equations show the relationship between these parameters [30]:

$$E = \frac{9BG}{3B + G}, \quad \nu = \frac{3B - 2G}{2(3B + G)}$$

Table 1 shows all elastic constants of γ -Fe, γ -Co, γ' -Fe₄N, CoFe₃N from the theoretical calculations. The mechanical stability of the crystal asks that B , c_{44} , and $(c_{11} - c_{12})$ are all positive constants [31]. According to them, the results in Table 1 imply that γ -Fe is not stable, whereas the γ' -Fe₄N and ^c(Co)^f(Fe₃)^b(N) are relatively stable, i.e., the insertion of N atoms into the Fe lattice can yields stable anti-perovskite crystal structure. In addition, the bulk modulus of γ' -Fe₄N is 167 GPa, which gives a deviation of 16% between our theoretical value and the experimental data (198 GPa) [32]. The elastic modulus of CoFe₃N compounds are substantially higher than γ' -Fe₄N, due to stronger directional bonding between Fe (f) and N and lower local magnetic moments for Co(f) atoms. Söderlind et al. [33] think that the reason for lower bulk modulus of γ' -Fe₄N compared to the ternary nitrides is likely of a magnetic nature: In SP phases, only one spin channel contributes to bonding.

An effective isotropic Poisson's ratio ν can be deduced as a measurement of the material to resist shear. It is also associated with the volume change during uniaxial deformation. Our calculated Poisson's ratio ν is given in Table 1 for all mentioned compounds. The highest value of Poisson's ratio ν is 0.65 for γ -Fe, which is not reliable due to the structural instability. It has been proved that 0.25 is the lower limit of ν for central-force solids and 0.5 is the upper limit, which corresponds to infinite elastic anisotropy. The high ν value (substantially higher than 0.25) for γ' -Fe₄N and ^c(Co)^f(Fe₃)^b(N) indicates that the interatomic forces in the compound are central. It has been suggested that the B/G ratio is related to the brittleness of the material with lower values suggesting that material is more brittle – Pugh [34] suggesting that when $B/G > 1.75$ the material has ductile features when $B/G < 1.75$ the material shows brittle character. Our calculated B/G value for γ' -Fe₄N and ^c(Co)^f(Fe₃)^b(N) is between 2.3 and 2.4 and it is higher than those of the constituent elements and the average value based on the rule of mixtures. The large B/G value due to the weak coupling between Fe–N and Fe–M layers (giving a small C_{44}) suggests rather ductile, as well as strong coupling within Fe–N layers (giving large bulk modulus) [14,15].

The results suggest that γ' -Fe₄N and ^c(Co)^f(Fe₃)^b(N) may therefore be ductile.

3.3. Electronic band structure

The SP electronic energy bands of the γ' -Fe₄N and CoFe₃N compounds are shown in Fig. 4. The bands corresponding to the spin-up (\uparrow) and spin-down (\downarrow) electrons spin apart are due to the exchange coupling between the electrons. In fact, the splitting width of the energy level indicates the strength of the exchange splitting, which reflects the strength of exchange interaction between the magnetic ions. In the present case the 45 bands near Fermi level are considered. The statistical average of exchange splitting is obtained from the band calculation, which is the result of self-consistent field calculations. Fig. 4(a) and (b) shows the exchange splittings $\Delta_x = E_{i\uparrow} - E_{i\downarrow}$ are positive. The statistical average value of exchange splitting is 1.29 eV for γ' -Fe₄N and 1.16 eV for CoFe₃N. The Curie temperature of the binary compound consisting of magnetic ions A and B can be expressed as $T_c = Z(n_A^2 J_{AA} + n_B^2 J_{BB} + 2n_A n_B J_{AB})/2k$, which had been described in ref. [35]. Because the N atoms are slightly SP, the expression can be approximately used for the γ' -Fe₄N and CoFe₃N compounds. According to the expression, the Curie temperature T_c decreases with decreasing exchange interaction between magnetic ions. The substitution of Co for Fe reduces the statistical average of exchange splitting and results in the decrease of T_c . In fact, the statistical average value of exchange splitting is 1.85 eV for γ -Fe, which is larger than that of γ' -Fe₄N and CoFe₃N. This indicates that the N insertion in the b sites of γ -Fe effectively screens the exchange interaction between the magnetic ions.

Fig. 4(a) and (b) shows that the changes of bands mainly appear near the Fermi level. The \downarrow bands cut the Fermi level, which is stronger 3d character than the \uparrow band. One notes that for γ' -Fe₄N, 0.6 eV and 0.8 eV gap appear for \uparrow states as a pseudogap in the present band structure, respectively. And for CoFe₃N, 0.3 eV and 0.4 eV gap appear for \uparrow states as a pseudogap in the present band structure, respectively. It is interesting to note that for CoFe₃N, the Fermi level lies in the up vicinity of the pseudogap for the \uparrow DOS, which is similar to that of γ' -Fe₄N. Note that the Fermi energy passes through the gap in the \uparrow DOS and the system behaves as half-metallic.

The TDOS of γ' -Fe₄N and CoFe₃N are shown in Fig. 5(a) and (b), respectively. The number of \uparrow electrons exceeds that of \downarrow electrons, which causes the distribution of DOS to be asymmetric, so that the ferromagnetism is induced. The PDOS between -8.5 and -5 eV in Fig. 5(a) and (b) are mostly due to N sp states, which have obviously different contribution to TDOS. This also implies different electron density contour of N ions in γ' -Fe₄N and CoFe₃N. The PDOS between -5 eV and 2 eV are mostly due to Fe 3d states for γ' -Fe₄N. Fig. 5 also shows the 3d electrons of a Co(c) atom give even more prominence to the contribution of the peak at E_f , i.e., near upon double than that of a Fe(f) atom. Two compounds show an obviously difference in the \downarrow DOS. These facts explain the differences in local moments discussed at the beginning of Sections 3 and 4. In fact, the N sp orbitals more strongly hybridize with Fe (f) 3d than Fe (c) 3d. And the feature

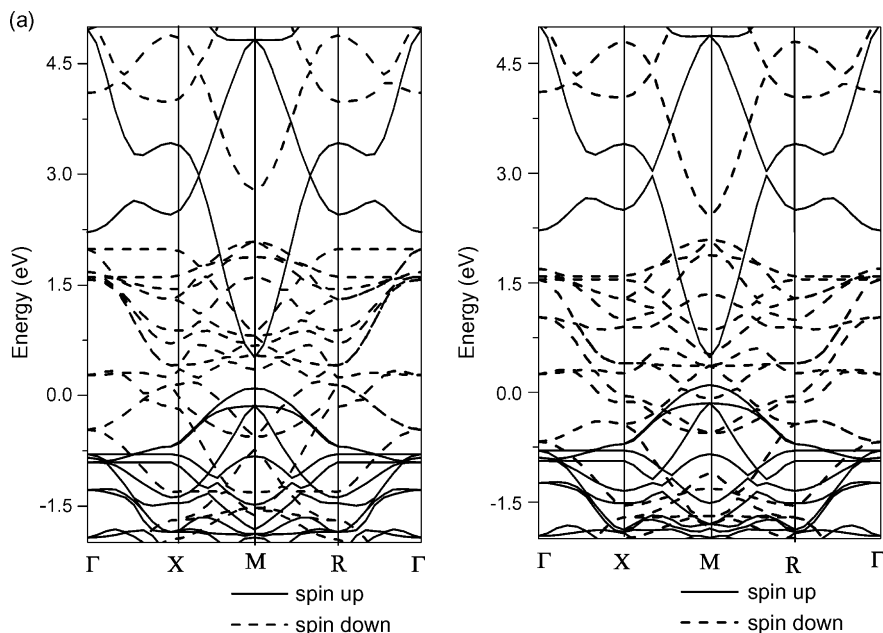


Fig. 4. Spin-polarized electronic energy band of (a) γ' -Fe₄N and (b) CoFe₃N in the selected highsymmetry directions in the Brillouin zone. The dashed line indicate the spin-up band, and the solid line indicate the spin-down band.

of local densities of metal atoms in γ' -Fe₄N is considerable different depending on the site. $N(E_f)$ presented in Table 1 is the TDOS per f.u. at E_f . $N(E_f)$ for CoFe₃N is 5.2 states/f.u., which is larger than 4.6 states/f.u. for γ' -Fe₄N. According to the generalized Stoner model condition [36], the Stoner factor $IN(E_f)$ of CoFe₃N is 1.92, which is larger than that of γ' -Fe₄N, indicating a stable ferromagnetism.

The effective ionic valences listed in Table 2 are defined to be the difference between the formal ionic charge and the Mulliken charge on the anion species in the crystal. It is also used as a measure of ionicity; a value of zero implies an ideal ionic bond while values greater than zero indicate increasing levels of covalency [26]. In fact, in γ' -Fe₄N and CoFe₃N compounds, the bonding types include covalent, ionic, and metallic character. The atoms at the cube corners, such as Fe(c) or Co, have a low net charge (−0.08 eV) while the Fe(c)–Fe(f) or Co(c)–Fe(f) bond has high overlap populations,

which indicates the bonds have obviously metallic character. We find that the numbers of valence electrons of Fe and Co are not integers, which implies that the cohesive bond is no longer purely metallic, and a nonmetallic component (ionic or covalent) has been added to it; they constitute a set of stable bonding orbitals. Table 2 shows the overlap populations for nearest neighbors in the crystal. Positive and negative values indicate bonding and antibonding states, respectively, and a value close to zero indicates that there is no significant interaction between the electronic populations of the two atoms. For example, in γ -Fe the overlap population between next-nearest Fe(f)–Fe(f) neighbor is −0.16 eV while in γ' -Fe₄N and CoFe₃N these populations are −0.61 and −0.65 eV, respectively. This indicates that the strong antibonding interaction between atoms in the second coordination shell is stronger in γ' -Fe₄N and CoFe₃N than in γ -Fe. A high overlap indicates a high degree of covalency

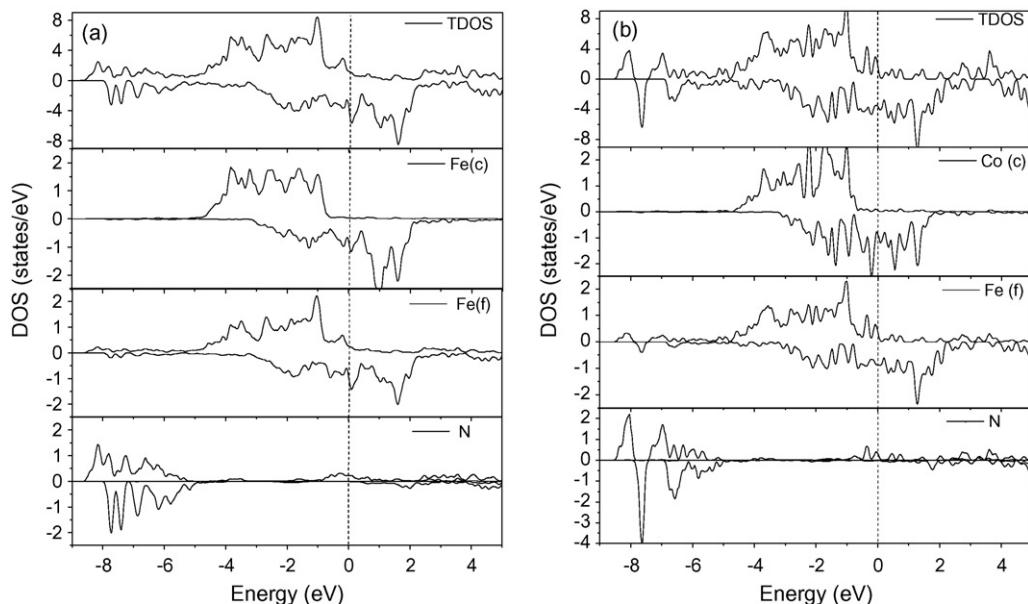


Fig. 5. Total and partial densities of states for (a) γ' -Fe₄N, (b) CoFe₃N. The Fermi energy is at zero.

Table 2Atomic Mulliken charges valence charges and the overlap populations of bonds in γ -Fe and iron nitride.

Material	Atom	Mulliken charge ($ e $)	Effective valence ($ e $)	bond	Overlap populations ($ e $)	bond length (Å)
γ -Fe	Fe	8	0	Fe–Fe	–0.16	2.547
γ' -Fe ₄ N	N	5.75	–0.75	N–Fe(f)	0.62	1.880
	Fe(f)	7.72	0.28	Fe(f)–Fe(f)	–0.61	2.659
	Fe(c)	8.08	–0.08	Fe(c)–Fe(f)	0.52	2.659
CoFe ₃ N	N	5.76	–0.76	N–Fe(f)	0.60	1.876
	Fe(f)	7.72	0.28	Fe(f)–Fe(f)	–0.65	2.653
	Co(c)	9.08	–0.08	Co(c)–Fe(f)	0.51	2.653

in the bond [26]. It is also found that the N–Fe(f) in γ' -Fe₄N has a slightly higher overlap than one in CoFe₃N, whereas the N–Fe(f) bond lengths has reverse trend, due to stronger interaction between Fe atoms than between Co and Fe atoms.

3.4. Magnetic properties

For γ' -Fe₄N at equilibrium volume, the calculated local magnetic moment are 2.96 μ_B and 2.24 μ_B for c and f site, respectively. The saturation magnetic moment per f.u. is 9.762 μ_B . The values are consistent with previous theoretical studies based on FPLAPW, i.e. 2.98 μ_B at c site and 2.23 μ_B at f site [37]. For CoFe₃N, the ground state is ferromagnetic and a comparison with γ' -Fe₄N nitride shows that the magnetic moment of Fe(f) atoms has a relative larger value than that of the same site in γ' -Fe₄N. Table 1 also shows a smaller magnetic moment of Co(c) atoms for CoFe₃N lead to a slightly low magnetic moment per formula unit. Comparing with other substituted iron nitrides, the substitution of Co gives the higher magnetic moment per formula unit and this is close to the value of the γ' -Fe₄N.

The f and c atoms are equivalent in γ -Fe, however, and nonequivalent in γ' -Fe₄N and CoFe₃N. It should be marked that the more distant c atoms from the N atom, Fe(c) for γ' -Fe₄N, Co(c) for CoFe₃N, have the larger 3d hole in the \downarrow states, which the \uparrow states of the sites are almost occupied. It is related to the bonding nature between N atom and surrounding Fe atoms. The electronic interference by the N atoms leads to the redistribution of the \downarrow electrons, yielding the variance of the moments on surrounding atoms. The 3d levels, especially the \downarrow states of f atoms are lowered through the hybridization with a part of the N 2p state located around the E_f and in turn the 3d \downarrow state of the c atoms are raised conversely. This electronic bonding feature is strongly responsible for the variation of the local magnetic moments of each atom site in the iron nitride system, which can be interpreted by the Mulliken charges and bond populations. As a result, the \downarrow electrons transfer from the c atoms to the f atoms. This means to reduce the difference in occupancy of the 3d \uparrow and \downarrow band for f atoms and to increase the difference in occupancy of the 3d \uparrow and \downarrow band for c atoms. That is, the N atoms in cubic lattice enhance the magnetic moments of the most distance c atoms, and decrease the magnetic moments of the nearest neighbor f atoms. Fig. 6 summarizes the mechanisms of the change of magnetic moment.

To investigate the sensitivity of the magnetic moment against lattice spacing for the γ' -Fe₄N and CoFe₃N, namely, to simulate pressure effect on the magnetic moment, we calculated the magnetic moments at several lattice parameters. Fig. 7 presents the behavior of the magnetic moments as a function of pressure for these nitrides (or equivalently with volume). Earlier investigation has shown that there is a transition from “low moment-low volume” to “high moment-large volume” for γ' -Fe₄N [38]. In CoFe₃N at low pressure, ferromagnetism remains practically unaltered with cobalt substitution, similar to the case of γ' -Fe₄N. At high pressure, drastic variations of the magnetic moment are observed including a transition from ferromagnetic to nonmagnetic state

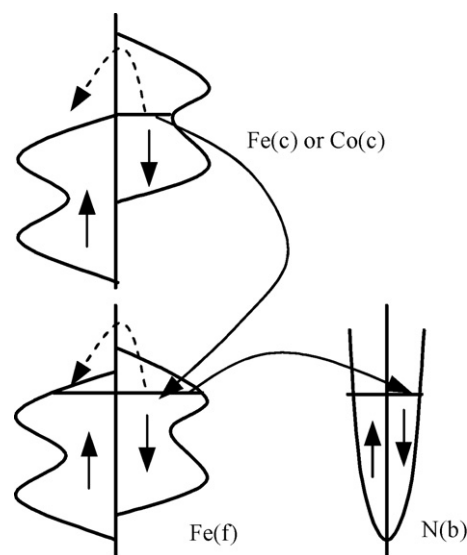


Fig. 6. The local DOS of face-centered and corner atoms change with the inclusion of the N atom, and electrons of the spin down states transfer in γ' -Fe₄N and CoFe₃N. The solid arrowheads denote the transfer of the 3d \downarrow electrons due to the N insertion. The dashed arrowheads denote the intra-atomic charge transfer that increases the magnetic moment, which relate to the distance between magnetic atoms.

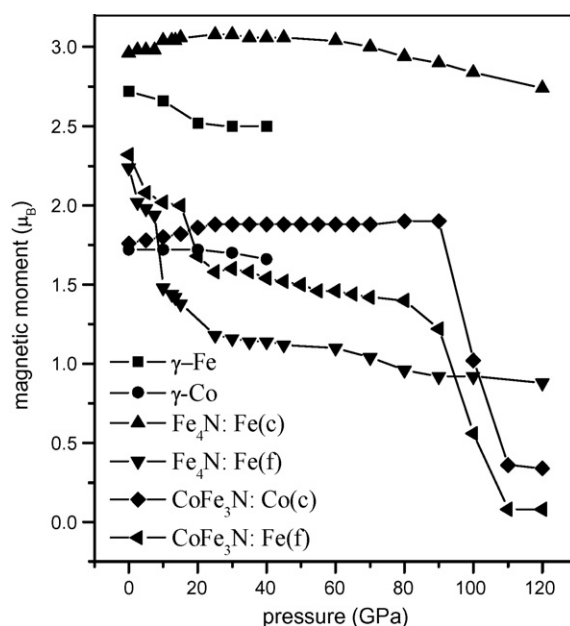


Fig. 7. The magnetic moments as a function of pressure at Fe(c) and Fe(f) for γ' -Fe₄N and Co(c) and Fe(f) for CoFe₃N.

for CoFe_3N . That is to say there is a collapse of the magnetic moment with extreme high pressure (>100 GPa) for CoFe_3N . The phenomenon is also observed in other substituted iron nitrides and is in good agreement with the experimental results on thermal expansion and forced magnetostriction, and applied pressure Mössbauer spectroscopy [32].

Fig. 7 shows that the effect of volume expansion is very great on the magnetic moment of f atoms, however, it is very small for that of c atoms. The increased distance between magnetic atoms leads to electrons transferring from the $3d \downarrow$ band to $3d \uparrow$ band. These mechanisms have been described in Fig. 6. Hence, contrary to the other metallic substitute (Ti), the substitution of Co for Fe have great magnetic moments at equilibrium volume, and the magnetic moments remain finite with the large range of volume, indicating the ferromagnetic stability. Thus, the CoFe_3N is ferromagnetic with a great magnetic per formula unit ($\cong 8.77 \mu_B$) at low pressure. However, at high pressure, the magnetic moments of Co(c) and three Fe(f) atoms have abruptly change to zero.

4. Conclusions

We have carried out first-principles total energy and electronic structure calculations for γ' - Fe_4N and CoFe_3N . The results show that the insertion of N atoms into the Fe lattice can yields stable anti-perovskite crystal structure and lead to the redistribution of the \downarrow electrons, thus the variance of the magnetic moments on surrounding atoms. CoFe_3N energetically prefers to yield ordered configurations for Co atoms occupying the c position. And the substitution of Co for Fe at c sites does hardly change the lattice constant, whereas it increases bulk modulus and could hardly changes the ductility. According to the generalized Stoner model condition, CoFe_3N is rather stable ferromagnetic. Moreover, we found the variation of the magnetic moment of f and c atoms is governed by a combining effect of two competitive factors, i.e., atomic volume expansion enhanced their magnetic moment, whereas hybridization with a part of the N 2p state reduced their magnetic moment. So the results show the further distant atoms from the N atom have the larger magnetic moment for γ' - Fe_4N and CoFe_3N , because the 3d levels, especially the \downarrow states of f atoms are lowered through the hybridization with a part of the N 2p state located around the E_f and in turn the $3d \downarrow$ state of the corner atoms are raised conversely, as a result, the \downarrow electrons transfer from the c atoms to the f atoms. Finally, SP calculations of the energy versus pressure show that the two compounds remain ferromagnetic at low pressure and have a transition to nonmagnetic at high pressure.

Acknowledgements

This work is supported by the New Century Excellent Talents in University (Grant No. NCET-04-0702), National Natural Science Foundation of China (Grant Nos. 50771047, 50371029). The authors thank L. Miao and S.W. Bie for valuable discussion.

References

- [1] C. Gao, W.D. Doyle, M. Shamsuzzoha, J. Appl. Phys. 73 (1993) 6579–6581.
- [2] L. Rissanen, M. Neubauer, K.P. Lieb, P. Schaaf, J. Alloys Compd. 274 (1996) 74–82.
- [3] D.L. Peng, T. Hihara, K. Sumiyama, J. Alloys Compd. 207 (2004) 377–383.
- [4] A.V. dos Santos, J.C. Krause, C.A. Kuhnen, Physica B 382 (2006) 290–299.
- [5] L.L. Wang, X. Wang, W.T. Zheng, et al., J. Alloys Compd. 443 (2007) 43–47.
- [6] L.L. Wang, W.T. Zheng, J. Gong, et al., J. Alloys Compd. 467 (2009) 1–5.
- [7] J.M.D. Coey, P.A.I. Smith, J. Magn. Magn. Mater. 200 (1999) 405–424.
- [8] L. Chen, J. Magn. Magn. Mater. 303 (2006) 1–5, 266.
- [9] J. von Appen, R. Dronskowski, Angew. Chem. Int. 44 (2005) 1205–1210.
- [10] R.N. Panda, N.S. Gajbhiye, J. Magn. Magn. Mater. 195 (1999) 396–405.
- [11] B. Siberchicot, S.F. Matar, L. Fournes, G. Demazeau, P. Hagenmuller, J. Solid State Chem. 84 (1990) 10–15.
- [12] H.Y. Wang, E.Y. Jiang, Z.W. Ma, Y.J. He, H.S. Huang, J. Phys.: Condens. Mater. 11 (1999) 989–995.
- [13] N.S. Gajbhiye, R.S. Ningthoujam, J. Weissmuüller, Hyperfine Interact. 156–157 (2004) 51–56.
- [14] D. Music, J.M. Schneider, Appl. Phys. Lett. 88 (2006) 1–3, 031914.
- [15] Z.J. Wu, J. Meng, Appl. Phys. Lett. 90 (2007) 1–3, 241901.
- [16] W. Kohn, L.J. Sham, Phys. Rev. A 140 (1965) A1133–A1138.
- [17] J.P. Perdew, Y. Wang, Phys. Rev. B 45 (1992) 13244–13249.
- [18] M.D. Segall, P.L.D. Lindan, M.J. Probert, C.J. Pickard, P.J. Hasnip, S.J. Clark, M.C. Payne, J. Phys.: Condens. Mater. 14 (2002) 2717–2744.
- [19] D. Vanderbilt, Phys. Rev. B 41 (1990) 7892–7895.
- [20] M.C. Long, W.M. Cai, Z.P. Wang, G.Z. Liu, Chem. Phys. Lett. 420 (2006) 71–76.
- [21] X.G. Ma, C.Q. Tang, J.Q. Huang, L.F. Hu, X. Xue, W.B. Zhou, Acta Phys. Sin. 55 (2006) 404–410.
- [22] T.H. Fischer, J. Almlöf, J. Phys. Chem. 96 (1992) 9768–9774.
- [23] B. Winkler, C. Pickard, V. Milman, Chem. Phys. Lett. 362 (2002) 266–270.
- [24] L. Bellaiche, D. Vanderbilt, Phys. Rev. B 61 (2000) 7877–7882.
- [25] D. Sanchez-Portal, E. Artacho, J.M. Soler, Solid State Commun. 95 (1995) 685–690.
- [26] M.D. Segall, R. Shah, C.J. Pickard, M.C. Payne, Phys. Rev. B 54 (1996) 16317–16320.
- [27] H. Jacobs, D. Rechenbach, U. Zachwieja, J. Alloys Compd. 227 (1995) 10–17.
- [28] J.S. Lord, J.G.M. Armitage, P.C. Riedi, S.F. Matar, G. Demazeau, J. Phys.: Condens. Mater. 6 (1994) 1779–1790.
- [29] D. Andriamandroso, S. Matar, G. Demazeau, L. Fournès, IEEE Trans. Magn. 29 (1993) 2–6.
- [30] L.D. Landau, E.M. Lifshitz, Theory of Elasticity, 3rd ed., Pergamon, Oxford, 1986.
- [31] M. Mattesini, S.F. Matar, Phys. Rev. B 65 (2002) 1–14, 075110.
- [32] C.L. Yang, M.M. Abd-Elmeguid, H. Micklitz, G. Michels, J.W. Otto, Y. Kong, D.S. Xue, F.S. Li, J. Magn. Magn. Mater. 151 (1995) L19–L23.
- [33] P. Söderlind, R. Ahuja, O. Eriksson, J.M. Wills, B. Johansson, Phys. Rev. B 50 (1994) 5918–5927.
- [34] S.F. Pugh, Philos. Mag. 45 (1954) 823–843.
- [35] S.V. Vonsovskii, Magnetism, Wiley, New York, 1997.
- [36] H.J. Nowak, O.K. Andersen, T. Fujiwara, O. Jepsen, P. Vargas, Phys. Rev. B 44 (1991) 3577–3598.
- [37] R. Coehoorn, G.H.O. Daalderop, H.J.F. Jansen, Phys. Rev. B 48 (1993) 3830–3834.
- [38] P. Mohn, S.F. Matar, J. Magn. Magn. Mater. 191 (1999) 234–240.